

Discrete-Time Repetitive Control for Multi-Harmonic Reference Trajectories with Arbitrary Frequency[★]

L. Marko^{*} M. Saxinger^{*} M. Bittner^{*} A. Steinboeck^{**}
A. Kugi^{*}

^{*} *Christian Doppler Laboratory for Model-Based Process Control in the Steel Industry, Automation and Control Institute, TU Wien, Austria, (e-mail: {marko, saxinger, kugi}@acin.tuwien.ac.at).*

^{**} *Automation and Control Institute, TU Wien, Austria (e-mail: steinboeck@acin.tuwien.ac.at)*

Abstract: In this work, a repetitive control approach for the tracking of harmonic reference trajectories in the presence of actuator backlash and sticking friction is presented. A spatial Fourier series formulation is utilized to obtain a learning law which is independent of the desired reference frequency. Subsequently, discrete-time averaging is employed, which results in a simple convergence criterion for the closed-loop system. Furthermore, all updates are calculated in a time-recursive manner, which avoids the necessity of large data windows and allows for a discrete-time implementation with a uniform sampling time. Finally, experimental results of a fully assembled spindle drive are presented. This demonstrates the effectiveness of the proposed control scheme as well as its suitability as an add-on strategy in existing positioning devices.

Keywords: Backlash, repetitive control, Fourier series, discrete-time implementation, averaging analysis

1. INTRODUCTION

In many applications of motion control it is necessary to generate accurate translational harmonic motions. Herein, the reference frequency is typically user-defined and time-variant. One possibility to realize such harmonic motions is the use of spindle drives. These drives are typically actuated by a stepper motor. This allows to realize trajectories with arbitrary low reference frequencies and a large range of motion. However, spindle drives typically exhibit backlash and static friction, which can significantly degrade the tracking performance, see, e.g., (Nordin and Gutman, 2002; Jukić and Perić, 2003).

To minimize tracking control errors due to backlash and frictional forces, different strategies have been pursued in the literature. A straightforward approach is to utilize a model-based compensation in the controller design. In this case, an appropriate backlash model is parametrized in advance or can even be adapted online, see (Cho et al., 2018; Mora et al., 2018; Lai et al., 2018). While these approaches can be used for arbitrary reference trajectories, their parametrization typically requires detailed knowledge of the internal states of the drive system. Thus, these methods are of limited use for commercially available spindle drive systems where only the input-output behavior is known based on measurements.

For periodic reference trajectories, repetitive control can be employed (Huang et al., 1998; Qin and Cai, 2001). Repetitive controllers iteratively learn the necessary control input to compensate for backlash solely based on the measured system output. Moreover, repetitive control can be easily added to existing drive control systems. Thus, this approach will be utilized in the current work.

Repetitive control is based on the internal model principle and proved effective in reducing the tracking error in the case of periodic reference trajectories (Li et al., 2004; Wang et al., 2009). However, as discussed by Ramos et al. (2011), the performance of conventional repetitive control degrades significantly if there is a mismatch between the characteristic frequency of the internal model and the frequency of the desired reference trajectory. Such a mismatch can occur if the reference frequency is changed during operation or, since most repetitive control schemes are implemented in discrete-time, if the period of the reference signal is not a multiple of the sampling time. In the past, different approaches have been proposed to deal with this problem of frequency mismatch. (Yu and Hu, 2000) suggested a method to redesign the control law online if the reference frequency changes. Steinbuch (2002) introduced additional memory elements to increase the robustness of repetitive control against uncertain reference frequencies. Olm et al. (2010) used non-uniform sampling of the time domain to keep the internal structure of the repetitive controller constant, even in case of varying reference frequencies. However, in general, these approaches are tied to a significant computational burden during online operation.

[★] The financial support by the Christian Doppler Research Association, the Austrian Federal Ministry for Digital and Economic Affairs, the National Foundation for Research, Technology and Development, and voestalpine Stahl GmbH is gratefully acknowledged.

To gain additional flexibility in case of time-variant reference frequencies, spatial repetitive control has been proposed by several authors. Here, the time t is mapped to the angular coordinate θ via the transformation

$$\theta(t) = \int_0^t 2\pi f_r(\tau) d\tau, \quad (1)$$

with the time-varying reference frequency $f_r(t)$. For $f_r(t) > 0$ this transformation is one-to-one and thus has an inverse $t = t(\theta)$. The main challenge in spatial repetitive control lies in its discrete-time implementation. To overcome this problem, (Abidi, 2014; Yao, 2015; Ramos et al., 2015) proposed uniform sampling over the spatial domain. In contrast, Yao et al. (2013) employed a period-based interpolation scheme over a non-uniform spatial grid. Huo et al. (2016) used a finite number of resonant filters, where the arbitrary reference frequency is regarded as a gain-scheduling parameter. While the method of Huo et al. (2016) can be easily implemented with uniform temporal sampling, controller tuning can be quite cumbersome if a high number of resonance filters is used. Furthermore, due to the purely time-recursive formulation, it is not clear how an appropriate anti-windup scheme can be realized with this approach.

To avoid such difficulties, the current work combines a Fourier series repetitive control approach with spatial repetitive control. In contrast to (Huang et al., 1998; Qin and Cai, 2001; Cheung and Hung, 2009), a time-recursive formulation is used in this work for the calculation of the Fourier coefficients. This approach requires neither the use of data windows nor an interpolation between temporal and spatial grids. This results in an efficient implementation with a uniform sampling time, even for very low reference frequencies.

The paper is organized as follows: The concept of spatial Fourier series repetitive control is introduced in Section 2. The resulting error dynamics of the closed-loop system is discussed in Section 2.1. In Section 2.2, a discrete-time averaging analysis of this error dynamics is carried out, which serves as a basis for a closed-loop stability criterion and for the tuning of the system. The implementation of the proposed algorithm is discussed in Section 2.3 and actuator constraints are considered in Section 2.4. The effectiveness of the proposed repetitive controller is demonstrated in Section 3 using the experimental setup shown in Fig. 1. Conclusions are given in Section 4.

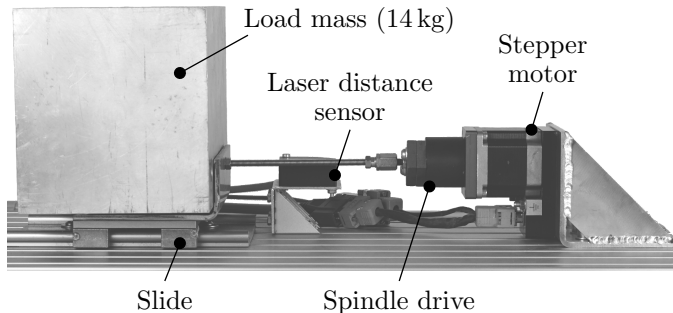


Fig. 1. Experimental setup.

2. SPATIAL FOURIER SERIES REPETITIVE CONTROL

In the following, the exponentially stable system

$$\dot{\mathbf{x}}(t) = \mathbf{A}\mathbf{x}(t) + \mathbf{b}_u u(\theta(t)) + \mathbf{b}_w w(\theta(t)) \quad (2a)$$

$$y(t) = \mathbf{c}^T \mathbf{x}(t), \quad (2b)$$

with the state $\mathbf{x} \in \mathbb{R}^m$, the initial condition $\mathbf{x}(0) = \mathbf{x}_0$, the inputs $u, w \in \mathbb{R}$, the output $y \in \mathbb{R}$, and the angular coordinate $\theta(t)$, as defined in (1), is considered. The disturbance input w describes a periodic perturbation and is represented by a Fourier series with N components in the form of

$$w(\theta) = \sum_{n=1}^N \boldsymbol{\sigma}_n^T(\theta) \mathbf{w}_n, \quad (3)$$

with the coefficients $\mathbf{w}_n \in \mathbb{R}^2$, and the harmonic functions

$$\boldsymbol{\sigma}_n^T(\theta) = [\cos(n\theta) \quad \sin(n\theta)]. \quad (4)$$

To compensate the effect of the disturbance w on the output y and to realize a desired reference trajectory

$$r(\theta) = \sum_{n=1}^N \boldsymbol{\sigma}_n^T(\theta) \mathbf{r}_n, \quad (5)$$

with $\mathbf{r}_n \in \mathbb{R}^2$, the control input u is parametrized in the form

$$u(\theta) = \sum_{n=1}^N \boldsymbol{\sigma}_n^T(\theta) \mathbf{Q}_n \mathbf{u}_n^p, \quad (6)$$

with the input parameters $\mathbf{u}_n \in \mathbb{R}^2$. The superscript p indicates the respective period, which is defined by $2\pi p \leq \theta \leq 2\pi(p+1)$, with $p = 0, 1, 2, \dots$. The period-based learning law for \mathbf{u}_n , with $n = 1, \dots, N$, is defined as

$$\mathbf{u}_n^{p+1} = \mathbf{u}_n^p + \mathbf{L}_n \Delta \mathbf{y}_n^p \quad (7)$$

with the spectral errors

$$\Delta \mathbf{y}_n^p = \frac{1}{\pi} \int_{2\pi p}^{2\pi(p+1)} \boldsymbol{\sigma}_n(\theta) (r(\theta) - y(t(\theta))) d\theta. \quad (8)$$

The performance of the closed-loop system is tuned by the gain matrices

$$\mathbf{L}_n = l_n \begin{bmatrix} \cos(\alpha_n) & \sin(\alpha_n) \\ -\sin(\alpha_n) & \cos(\alpha_n) \end{bmatrix} \quad (9a)$$

$$\mathbf{Q}_n = q_n \begin{bmatrix} \cos(\beta_n) & \sin(\beta_n) \\ -\sin(\beta_n) & \cos(\beta_n) \end{bmatrix}, \quad (9b)$$

with the gains $l_n, q_n > 0$ and the angles α_n and β_n .

Remark 1. Constant perturbations can be efficiently rejected by integral feedback and are therefore not further considered in the proposed control scheme. However, a corresponding extension of the algorithm is straightforward and thus, is omitted for the sake of brevity.

2.1 Error dynamics

As a preparation for formulating the closed-loop error dynamics, the steady-state of the system is computed. Herein, steady-states are indicated by the superscript s . In the following, an arbitrary constant reference frequency f_r^s , with a corresponding period $T_r^s = 1/f_r^s$, and constant reference parameters \mathbf{r}_n^s and disturbance parameters \mathbf{w}_n^s are assumed. Thus, (1) reduces to

$$\dot{\theta}^s(t) = 2\pi f_r^s t. \quad (10)$$

From (7), the steady-state values for the spectral errors result in $\Delta \mathbf{y}_n^s = \mathbf{0}$, if a steady-state control input $\mathbf{u}_n^{p+1} = \mathbf{u}_n^p = \mathbf{u}_n^s$ is applied. Consequently, (2)-(6) and the transfer functions

$$G_u(s) = \mathbf{c}^T (s\mathbf{I} - \mathbf{A})^{-1} \mathbf{b}_u \quad (11a)$$

$$G_w(s) = \mathbf{c}^T (s\mathbf{I} - \mathbf{A})^{-1} \mathbf{b}_w \quad (11b)$$

with the Laplace variable s , yield the steady-state condition

$$\mathbf{r}_n^s = \begin{bmatrix} \operatorname{Re}(G_u(jn\omega_r^s)) & \operatorname{Im}(G_u(jn\omega_r^s)) \\ -\operatorname{Im}(G_u(jn\omega_r^s)) & \operatorname{Re}(G_u(jn\omega_r^s)) \end{bmatrix} \mathbf{Q}_n \mathbf{u}_n^s + \begin{bmatrix} \operatorname{Re}(G_w(jn\omega_r^s)) & \operatorname{Im}(G_w(jn\omega_r^s)) \\ -\operatorname{Im}(G_w(jn\omega_r^s)) & \operatorname{Re}(G_w(jn\omega_r^s)) \end{bmatrix} \mathbf{w}_n^s, \quad (12)$$

with $\omega_r^s = 2\pi f_r^s$ for the steady-state input parameters \mathbf{u}_n^s , $n = 1, \dots, N$. Based on (2), the stationary state trajectory $\mathbf{x}^s(t)$ is thus given by

$$\dot{\mathbf{x}}^s(t) = \mathbf{A}\mathbf{x}^s(t) + \mathbf{b}_u \sum_{n=1}^N \sigma_n^T(t) \mathbf{Q}_n \mathbf{u}_n^s + \mathbf{b}_w w(\theta^s(t)) \quad (13a)$$

$$r(\theta^s(t)) = \mathbf{c}^T \mathbf{x}^s(t), \quad (13b)$$

with the abbreviation $\sigma_n(t) = \sigma_n(\theta^s(t))$.

Remark 2. From (12), it becomes clear that $G_u(jn\omega_r^s) \neq 0$ must hold for all n to obtain a unique solution for \mathbf{u}_n^s . As will be demonstrated by the analysis in Section 2.2, this is a necessary condition for convergence of the proposed learning law.

Let the difference between current values and steady-state values be indicated by $(\tilde{\cdot})$, i.e., $\tilde{\mathbf{u}}_n^p = \mathbf{u}_n^p - \mathbf{u}_n^s$, $\tilde{\mathbf{x}}(t) = \mathbf{x}(t) - \mathbf{x}^s(t)$ and $\tilde{y}(t) = y(t) - r(t)$. Hence, the error dynamics in terms of (2) and (7) can be written as

$$\dot{\tilde{\mathbf{x}}}(t) = \mathbf{A}\tilde{\mathbf{x}}(t) + \mathbf{b}_u \sum_{n=1}^N \sigma_n^T(t) \mathbf{Q}_n \tilde{\mathbf{u}}_n^p \quad (14a)$$

$$\tilde{y}(t) = \mathbf{c}^T \tilde{\mathbf{x}}(t), \quad (14b)$$

and

$$\tilde{\mathbf{u}}_n^{p+1} = \tilde{\mathbf{u}}_n^p + \mathbf{L}_n \Delta \mathbf{y}_n^p, \quad (15)$$

respectively.

Combining (15) with (14) results in a system which evolves on two time axes given by the continuous time t and the period index p , respectively. To analyze the system behavior in a systematic way, the state error dynamics is formulated in a period-based description. To this end, the discrete-time value of $\tilde{\mathbf{x}}(t)$ at the start of period p is defined by $\tilde{\mathbf{x}}^p = \tilde{\mathbf{x}}(pT_r^s)$ and its evolution is governed by

$$\tilde{\mathbf{x}}^{p+1} = \Phi_{xx} \tilde{\mathbf{x}}^p + \sum_{n=1}^N \Phi_{xn} \tilde{\mathbf{u}}_n^p, \quad (16)$$

with

$$\Phi_{xx} = e^{\mathbf{A}T_r^s}, \quad \Phi_{xn} = \int_0^{T_r^s} e^{\mathbf{A}(T_r^s-t)} \mathbf{b}_u \sigma_n^T(t) dt \mathbf{Q}_n. \quad (17)$$

Furthermore, the time-dependent output error $\tilde{y}(t)$ during the interval $t \in [pT_r^s, (p+1)T_r^s]$ can be written as

$$\tilde{y}(t) = \mathbf{c}^T e^{\mathbf{A}(t-pT_r^s)} \tilde{\mathbf{x}}^p + \sum_{n=1}^N \left(\int_0^{t-pT_r^s} \mathbf{c}^T e^{\mathbf{A}(t-pT_r^s-\tau)} \mathbf{b}_u \sigma_n^T(\tau) d\tau \right) \mathbf{Q}_n \tilde{\mathbf{u}}_n^p. \quad (18)$$

With (10) and (18), the spectral errors $\Delta \mathbf{y}_n^p$ according to (8) follow in the form

$$\Delta \mathbf{y}_n^p = \Phi_{nx} \tilde{\mathbf{x}}^p + \sum_{m=1}^N \Phi_{nm} \tilde{\mathbf{u}}_m^p, \quad (19)$$

with the abbreviations

$$\Phi_{nx} = -\frac{2}{T_r^s} \int_0^{T_r^s} \sigma_n(t) \mathbf{c}^T e^{\mathbf{A}t} dt \quad (20a)$$

$$\Phi_{nm} = -\frac{2}{T_r^s} \int_0^{T_r^s} \sigma_n(t) \int_0^t \mathbf{c}^T e^{\mathbf{A}(t-\tau)} \mathbf{b}_u \sigma_m^T(\tau) d\tau dt \mathbf{Q}_m. \quad (20b)$$

Combining (15), (16) and (19) results in the period-based closed-loop error dynamics

$$\begin{bmatrix} \tilde{\mathbf{x}}^{p+1} \\ \tilde{\mathbf{u}}_1^{p+1} \\ \vdots \\ \tilde{\mathbf{u}}_N^{p+1} \end{bmatrix} = \begin{bmatrix} \Phi_{xx} & \Phi_{x1} & \dots & \Phi_{xN} \\ \mathbf{L}_1 \Phi_{1x} & \mathbf{I} + \mathbf{L}_1 \Phi_{11} & \dots & \mathbf{L}_1 \Phi_{1N} \\ \vdots & \vdots & \ddots & \vdots \\ \mathbf{L}_N \Phi_{Nx} & \mathbf{L}_N \Phi_{N1} & \dots & \mathbf{I} + \mathbf{L}_N \Phi_{NN} \end{bmatrix} \begin{bmatrix} \tilde{\mathbf{x}}^p \\ \tilde{\mathbf{u}}_1^p \\ \vdots \\ \tilde{\mathbf{u}}_N^p \end{bmatrix}, \quad (21)$$

where $\mathbf{I} \in \mathbb{R}^{2 \times 2}$ is the identity matrix. Although (21) is a discrete-time linear time-invariant system, a general stability analysis would be rather involved due to the fully occupied dynamic matrix as well as the possibly high number of states. However, additional insights can be gained by the discrete-time averaging analysis described in the following section.

2.2 Averaging analysis

The averaging analysis of the error dynamics starts with a reformulation of the gain matrices in (9) as $\mathbf{L}_n = \varepsilon \bar{\mathbf{L}}_n$, with a small perturbation parameter $\varepsilon > 0$. The combination of (15), (16) and (18) can thus be rewritten in the form of

$$\tilde{\mathbf{x}}^{p+1} = \Phi_{xx} \tilde{\mathbf{x}}^p + \mathbf{H} \mathbf{z}^p \quad (22a)$$

$$\mathbf{z}^{p+1} = \mathbf{z}^p + \varepsilon \mathbf{f}(\tilde{\mathbf{x}}^p, \mathbf{z}^p), \quad (22b)$$

with $\mathbf{z}^p = [(\tilde{\mathbf{u}}_1^p)^T \dots (\tilde{\mathbf{u}}_N^p)^T]^T$, $\mathbf{H} = [\Phi_{x1} \dots \Phi_{xN}]$ and

$$\mathbf{f}(\tilde{\mathbf{x}}^p, \mathbf{z}^p) = \begin{bmatrix} \bar{\mathbf{L}}_1 \Delta \mathbf{y}_1^p \\ \vdots \\ \bar{\mathbf{L}}_N \Delta \mathbf{y}_N^p \end{bmatrix}. \quad (23)$$

The period-based error dynamics (22) is in standard form for discrete-time mixed-timescale averaging analysis according to Theorem 2.2.3 in (Bai et al., 1988). Given that ε is sufficiently small, the objective of the averaging analysis is to find an averaged representation of (22) in the form

$$\mathbf{z}_{\text{av}}^{p+1} = \mathbf{z}_{\text{av}}^p + \varepsilon \mathbf{f}_{\text{av}}(\mathbf{z}_{\text{av}}^p), \quad (24)$$

with the averaged state \mathbf{z}_{av}^p and the averaged function \mathbf{f}_{av} . The averaged system (24) is easier to analyze than the error dynamics in (22). Furthermore, if Φ_{xx} is exponentially stable, Theorem 2.2.4 in (Bai et al., 1988) guarantees the exponential stability of (22) and thus (21), if (24) is exponentially stable and if ε is chosen sufficiently small.

Since \mathbf{f} is linear in the spectral errors $\Delta \mathbf{y}_n^p$, the calculation of \mathbf{f}_{av} can be simplified by evaluating the average spectral errors according to

$$\Delta \mathbf{y}_{\text{av},n}^p = -\lim_{M \rightarrow \infty} \frac{2}{MT_r^s} \int_0^{MT_r^s} \sigma_n(t) \tilde{y}(t) dt, \quad (25)$$

where \mathbf{z}^p in (23) is replaced by \mathbf{z}_{av}^p , which is kept constant for the limit case $M \rightarrow \infty$. To evaluate (25), $\tilde{y}(t)$ is split in to a transient component $\tilde{y}_{\text{tr}}(t)$ and the steady state component $\tilde{y}_{\text{ss}}(t)$ according to $\tilde{y}(t) = \tilde{y}_{\text{tr}}(t) + \tilde{y}_{\text{ss}}(t)$ with

$$\tilde{y}_{\text{ss}}(t) = \sum_{n=1}^N \sigma_n^T(t) \mathbf{G}_n \mathbf{Q}_n \tilde{\mathbf{u}}_{\text{av},n}^p, \quad (26)$$

$\tilde{\mathbf{u}}_{\text{av},n}^p$ as the n -th entry in \mathbf{z}_{av}^p and the abbreviation

$$\mathbf{G}_n = \begin{bmatrix} \text{Re}(G_u(jn\omega_r^s)) & \text{Im}(G_u(jn\omega_r^s)) \\ -\text{Im}(G_u(jn\omega_r^s)) & \text{Re}(G_u(jn\omega_r^s)) \end{bmatrix}. \quad (27)$$

Due to the exponential stability of (2), $y_{\text{tr}}(t)$ is bounded and vanishes for $t \rightarrow \infty$. Thus, (25) reduces to

$$\Delta \mathbf{y}_{\text{av},n}^p = -\frac{2}{T_r^s} \sum_{m=1}^N \left(\int_0^{T_r^s} \sigma_n(t) \sigma_m^T(t) dt \right) \mathbf{G}_m \mathbf{Q}_m \mathbf{u}_{\text{av},m}^p, \quad (28)$$

and with

$$\int_0^{T_r^s} \sigma_n(t) \sigma_m^T(t) dt = \begin{cases} \mathbf{I}, & n = m \\ \mathbf{0}, & \text{else} \end{cases} \quad (29)$$

this results in

$$\Delta \mathbf{y}_{\text{av},n}^p = -\mathbf{G}_n \mathbf{Q}_n \tilde{\mathbf{u}}_{\text{av},n}^p. \quad (30)$$

Based on (15) and (30), the components of (24) follow as

$$\tilde{\mathbf{u}}_{\text{av},n}^{p+1} = (\mathbf{I} - \mathbf{L}_n \mathbf{G}_n \mathbf{Q}_n) \tilde{\mathbf{u}}_{\text{av},n}^p, \quad (31)$$

which are exponentially stable iff

$$\rho(\mathbf{I} - \mathbf{L}_n \mathbf{G}_n \mathbf{Q}_n) < 1. \quad (32)$$

Here, $\rho(\mathbf{M})$ denotes the spectral radius of the matrix \mathbf{M} . Due to the duality between complex numbers and 2×2 matrices with the shape of (9) and (27), the stability condition (32) can be formulated in the complex plane as

$$|1 - \lambda_n G_u(jn\omega_r^s) \kappa_n| < 1, \quad (33)$$

with

$$\lambda_n = l_n (\cos(\alpha_n) + j \sin(\alpha_n)) \quad (34a)$$

$$\kappa_n = q_n (\cos(\beta_n) + j \sin(\beta_n)) \quad (34b)$$

for all $n = 1, 2, \dots, N$.

The stability criterion (33) for the closed-loop system resembles the monotonic convergence criterion in optimal iterative learning control, see (Ge et al., 2018). Thus, $\lambda_n \kappa_n$ can be interpreted as a non-causal filter evaluated at the frequency $n\omega_r^s$. Based on (33), the optimal choice for the tuning gains is $\lambda_n \kappa_n = G_u^{-1}(jn\omega_r^s)$. The specific choice of λ_n and κ_n depends on the structure of the considered plant (2). For the experimental setup in Fig. 1, this will be discussed in detail in Section 3.

2.3 Discrete-time implementation

To implement the proposed algorithm on a discrete-time grid $t_k = T_s k$ with a constant sampling time T_s and $k = 0, 1, \dots$, (1) and (8) have to be discretized in time. Using the explicit Euler scheme, the discrete-time version of (1) follows in the form

$$\theta_{k+1} = \left(\theta_k + 2\pi T_s f_r(t_k) \right) \bmod 2\pi. \quad (35)$$

Herein, the modulo operation is used to avoid an overflow during online operation. Furthermore, with $f_r(t) > 0$, it allows to easily determine the first time index k of each period p by checking for $\theta_k - \theta_{k-1} \leq 0$.

With the the use of (35), and the explicit Euler scheme, the discrete-time version of (8) can be written in the recursive form

$$\Delta \mathbf{y}_{n,k+1} = \Delta \mathbf{y}_{n,k} - 2T_s f_r(t_k) \sigma_n(\theta_k) \tilde{y}_k. \quad (36)$$

Herein, $\Delta \mathbf{y}_{n,k}$ is recursively updated on a sample-to-sample basis until $\theta_{k+1} - \theta_k \leq 0$ is fulfilled. In this case, $\Delta \mathbf{y}_{n,k+1}$ is used as the period-based spectral error $\Delta \mathbf{y}_n^p$ in the learning law (7), which is executed once per reference period p . Thereafter, $\Delta \mathbf{y}_{n,k+1}$ is reset to zero to start the recursive integration for the next period.

The described recursive computation distributes the computational load of evaluating (8) equally over all sampling instances. Thus, the presented implementation is independent of the number of samples per period and avoids the computation of the fast Fourier transform for a high and possibly varying number of samples. Compared to (Huang et al., 1998; Cheung and Hung, 2009; Espíndola-López et al., 2016), this results in an implementation which also allows for very long reference periods with a high number of samples.

2.4 Actuator constraints

So far the repetitive control scheme was discussed without any restrictions on the control input. An advantage of utilizing a period-based update law is that the control input over the next reference period is known in advance. Thus, it is possible to look ahead and check for violations of actuator constraints, like the box constraints

$$-\bar{u} \leq u(t) \leq \bar{u}, \quad (37)$$

with the maximum control input \bar{u} . Consider the prediction of the unconstrained spectral components according to

$$\hat{\mathbf{u}}_n^{p+1} = \mathbf{u}_n^p + \mathbf{L}_n \Delta \mathbf{y}_n^p. \quad (38)$$

Before the learning update according to (7) is carried out, the corresponding input trajectory for the next period is predicted in the form

$$\hat{u}_i^{p+1} = \sum_{n=1}^N \sigma_n^T(i\delta_\theta) \mathbf{Q}_n \hat{\mathbf{u}}_n^{p+1} \quad (39)$$

on a suitably chosen angular grid $\{\delta_\theta, 2\delta_\theta, \dots, 2\pi\}$ with P points, the step size $\delta_\theta = 2\pi/P$ and the index $i = 1, \dots, P$. Based on this prediction, the Fourier coefficients for the next period are scaled in the form

$$\mathbf{u}_n^{p+1} = \eta^{p+1} \hat{\mathbf{u}}_n^{p+1}, \quad (40)$$

with the reduction factor

$$\eta^{p+1} = \min \left(1, \bar{u} / \max_i \left(|\hat{u}_i^{p+1}| \right) \right). \quad (41)$$

Remark 3. If the actuator constraints are active, i.e. $|u(t)| = \bar{u}$ for some t , perfect output tracking characterized by $y(t) = r(t)$ is no longer possible. However, since $u(t)$ is bounded, and because (2) is exponentially stable, all system states are guaranteed to be bounded even in this case.

3. EXPERIMENTAL RESULTS

The effectiveness of the proposed control scheme is demonstrated by measurements carried out on the experimental rig shown in Fig. 1. The setup consists of a 14 kg mass mounted on a slide which is moved by the commercially

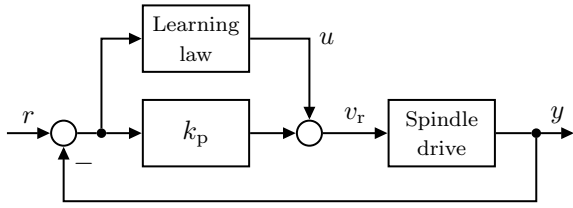


Fig. 2. Control structure in the experiment.

Table 1. Numerical values of the controller parameters used in experiments.

$\lambda_1 = (15 + 15j) \cdot 10^{-6}$	$\lambda_5 = (1 + 10j) \cdot 10^{-6}$	$\lambda_9 = 1 \cdot 10^{-6}$
$\lambda_2 = (5 + 20j) \cdot 10^{-6}$	$\lambda_6 = (1 + 12j) \cdot 10^{-6}$	$\lambda_{10} = 1 \cdot 10^{-6}$
$\lambda_3 = (5 + 15j) \cdot 10^{-6}$	$\lambda_7 = (1 + 14j) \cdot 10^{-6}$	$P = 200$
$\lambda_4 = (2 + 12j) \cdot 10^{-6}$	$\lambda_8 = (1 + 16j) \cdot 10^{-6}$	$k_p = 50/s$

available spindle drive Gunda Colibri-L KE17. The spindle drive accepts velocity commands (steps per sample time) and allows linear motions in the range $-5 \dots 5$ mm. The position of the mass y is measured by a laser displacement sensor Welotec OWLE 5060 S1. A dSPACE real-time platform DS1103 is utilized to execute the control algorithm within a sampling time of $T_s = 1$ ms.

Since the spindle drive is used as an off-the-shelf component, internal signals like motor currents or voltages can not be accessed. Moreover, there is a significant backlash in the spindle drive. In the following, the system behavior is described by the simple model

$$\dot{y}(t) = v_r(t) + w(\theta(t)), \quad (42)$$

with the reference speed $v_r(t)$. This plant model is not exponentially stable as required for the stability analysis in Section 2. Thus, a proportional feedback controller with the gain k_p is used to obtain an exponentially stable system. Together with $u(\theta)$ according to (6) this results in the control input

$$v_r(t) = u(\theta(t)) + k_p(r(t) - y(t)). \quad (43)$$

The resulting control structure is shown in Fig. 2.

Due to the integrating behavior of (42), the gain matrix in (6) is chosen as

$$\mathbf{Q}_n = 2\pi n f_r(t) \mathbf{I} \quad (44)$$

for $n = 1, \dots, N$. With this choice, the output $u(\theta)$ scales with the reference frequency. Thus, according to (42), the coefficients \mathbf{u}_n remain approximately constant for small changes of the reference frequency. This leads to a better tracking performance in the case of a time-varying frequency. Following the discussion after (32), the optimal choice for \mathbf{L}_n would be $\mathbf{L}_n = \varepsilon \mathbf{Q}_n^{-1} \mathbf{G}_n^{-1}$, with a sufficiently small gain parameter $\varepsilon > 0$. However, since (42) is only a simple model of the real plant behavior, \mathbf{G}_n is not accurately known and a better performance can be achieved by manual tuning of \mathbf{L}_n during the experiments. The resulting values for \mathbf{L}_n are summarized in Table 1 in the form (34a). The repetitive controller is first tuned for $N = 1$ by increasing l_1 and α_1 until a suitable convergence speed is observed. Then, the order of the repetitive controller is successively increased by one and the additional gain matrix \mathbf{L}_N is tuned analogous to \mathbf{L}_1 .

The objective of the following experiments was to realize a sinusoidal reference trajectory

$$r(t) = R \sin(\theta(t)) = \boldsymbol{\sigma}_1^T(\theta(t)) \mathbf{r}_1, \quad (45)$$

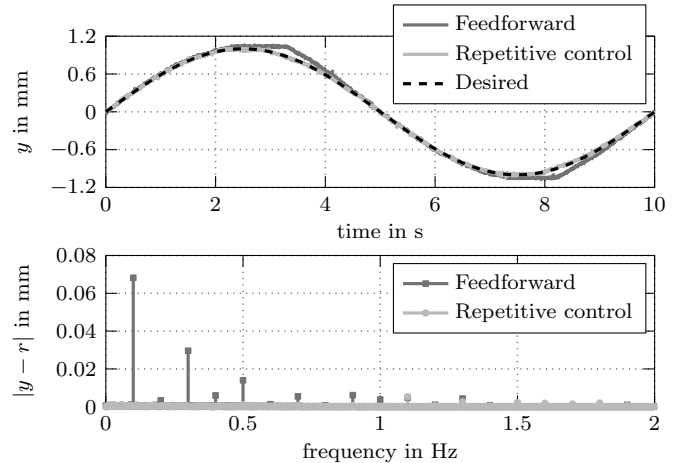


Fig. 3. Steady-state results for a sinusoidal reference with $R = 1$ mm, $f_r = 0.1$ Hz and $N = 10$ in the repetitive controller.

with $\mathbf{r}_1 = [0 \ R]^T$ and $\theta(t)$ according to (1). Thus, based on (42), the first spectral component of the input is initialized as $\mathbf{u}_1^0 = [R \ 0]^T$. All other components \mathbf{u}_n^0 , with $n = 2, \dots, N$, are set to zero. This initial values may be considered as ideal model-based feedforward input and will be compared to the proposed repetitive control scheme.

A reference trajectory with $R = 1$ mm and $f_r = 0.1$ Hz is considered in the first experiment. Although this results in 10^4 samples per reference period, this high number of samples does not constitute a problem regarding real-time execution due to the time recursive implementation discussed in Section 2.3. Fig. 3 shows the steady-state results for the first experiment. The combination of the feedforward controller and the proportional feedback controller results in a reasonable tracking performance over large portions of the reference trajectory. However, when the direction of movement changes, the tracking performance significantly deteriorates due to backlash. This deviation is also visible in the error spectrum shown in Fig. 3. In comparison, the proposed repetitive controller with $N = 10$ components achieves an almost perfect rejection of all spectral error components up to 1 Hz.

To demonstrate the effects of actuator constraints, Fig. 4 shows results from a second experiment with different values for R and $f_r = 10$ Hz. In this experiment, $N = 3$ already leads to a sufficiently good tracking performance, at least for a reference trajectory with $R = 1$ mm. For $R = 1.5$ mm, the control input $u(\theta)$ would violate the box constraints (37) with $\bar{u} = 75$ mm/s. In this case, the control input is restricted to $|u| \leq 75$ mm/s, cf. Fig. 4. However, due to the active input constraint, perfect tracking of the reference trajectory is no longer possible.

Results from a third experiment with $R = 1$ mm and a time-varying reference frequency f_r are shown in Fig. 5. The control starts at the corresponding steady-state with $f_r = 1$ Hz. It should be noted that the time-varying reference frequency is also considered in the feedforward control via (1) and the frequency dependent choice of \mathbf{Q}_n according to (44). Nonetheless, the proposed repetitive controller still leads to a significant reduction of the tracking error compared to the combination of feedforward and proportional control.

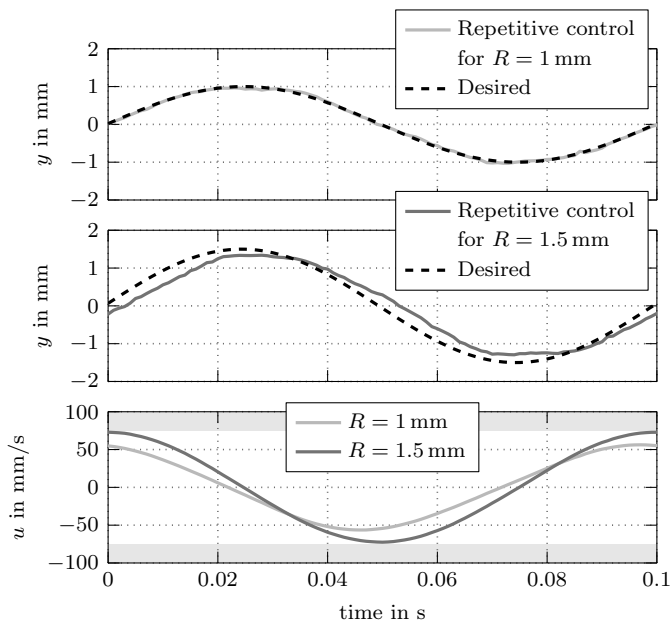


Fig. 4. Steady-state results for a sinusoidal reference with different values R , constant frequency $f_r = 10$ Hz, and $N = 3$. The maximal control input is $\bar{u} = 75$ mm/s.

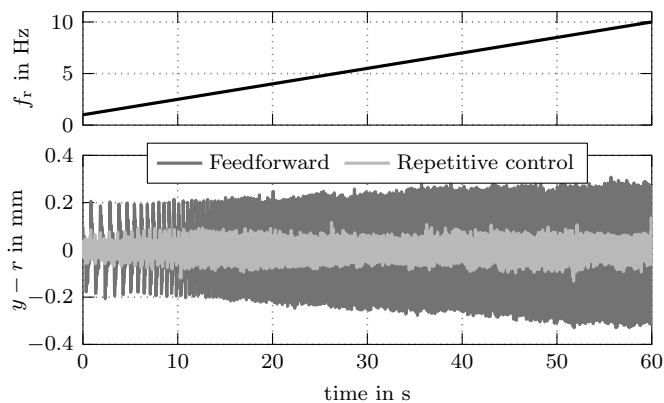


Fig. 5. Output error for a time-varying reference frequency f_r with $N = 3$ in the repetitive controller.

4. CONCLUSIONS

This work presented a backlash and friction compensation scheme for periodic reference trajectories with arbitrary reference frequency based on spatial Fourier series repetitive control. Discrete-time averaging analysis was applied to obtain a simple stability criterion that can assist in the parametrization of the proposed algorithm. Due to the time-recursive calculation of the update law, the algorithm can be easily realized with a constant sampling time even for reference periods with a high number of samples per period. Finally, the presented experimental results demonstrate the effectiveness of the proposed repetitive controller, even if the control input is constrained.

REFERENCES

Abidi, K., 2014. Spatial periodic adaptive control approach for rotary systems in sampled time. *International Journal of Robust and Nonlinear Control* 24 (7), 1177–1188.
 Bai, E., Fu, L., Sastry, S. S., 1988. Averaging analysis for discrete time and sampled data adaptive systems. *IEEE Transactions on Circuits and Systems* 35 (2), 137–148.

Cheung, J. W. F., Hung, Y. S., 2009. Robust learning control of a high precision planar parallel manipulator. *Mechatronics* 19 (1), 42–55.
 Cho, G. R., Kim, S.-T., Kim, J., 2018. Backlash compensation for accurate control of biopsy beedle manipulators having long cable transmission. *International Journal of Precision Engineering and Manufacturing* 19 (5), 675–684.
 Espíndola-López, E., Gómez-Espinosa, A., Carrillo-Serrano, R. V., Jáuregui-Correa, J. C., 2016. Fourier series learning control for torque ripple minimization in permanent magnet synchronous motors. *Applied Sciences* 6 (9), 254.
 Ge, X., Stein, J. L., Ersal, T., 2018. Frequency-domain analysis of robust monotonic convergence of norm-optimal iterative learning control. *IEEE Transactions on Control Systems Technology* 26 (2), 637–651.
 Huang, W., Cai, L., Tang, X., 1998. Adaptive repetitive output feedback control for friction and backlash compensation of a positioning table. In: *Proc. of the 37th IEEE Conference on Decision and Control*. Vol. 2. Tampa, FL, USA, pp. 1250–1251.
 Huo, X., Tong, X.-G., Liu, K.-Z., Ma, K.-M., 2016. A compound control method for the rejection of spatially periodic and uncertain disturbances of rotary machines and its implementation under uniform time sampling. *Control Engineering Practice* 53, 68–78.
 Jukić, T., Perić, N., Sep. 2003. A comparative study of backlash compensation methods. In: *Proc. of the 2003 European Control Conference*. Cambridge, UK, pp. 3261–3266.
 Lai, G., Wen, C., Liu, Z., Zhang, Y., Chen, C. L. P., Xie, S., 2018. Adaptive inverse compensation for actuator backlash with piecewise time-varying parameters. *International Journal of Control* 91 (2), 337–345.
 Li, C., Zhang, D., Zhuang, X., Sep. 2004. A survey of repetitive control. In: *Proc. of the 2004 IEEE/RSJ International Conference on Intelligent Robots and Systems*. Vol. 2. Sendai, JPN, pp. 1160–1166.
 Mora, C. M., Rosas, A. D., Rascon, C. R., Cuesta, G. R., 2018. Robust output control of an uncertain underactuated 2DOF mass-spring-damper system with backlash based on active disturbance rejection control structure. *Mathematical Problems in Engineering* 2018, 1–10.
 Nordin, M., Gutman, P.-O., 2002. Controlling mechanical systems with backlash - a survey. *Automatica* 38 (10), 1633–1649.
 Olm, J. M., Ramos, G. A., Costa-Castelló, R., 2010. Adaptive compensation strategy for the tracking/rejection of signals with time-varying frequency in digital repetitive control systems. *Journal of Process Control* 20 (4), 551–558.
 Qin, W., Cai, L., Jun. 2001. A frequency domain iterative learning control for low bandwidth system. In: *Proc. of the 2001 American Control Conference*. Arlington, VA, USA, pp. 1262–1267.
 Ramos, G., Olm, J. M., Costa-Castelló, R., 2011. A survey of repetitive control in varying frequency conditions. *Ingeniería e Investigación* 31, 29–37.
 Ramos, G. A., Cortés-Romero, J., Coral-Enriquez, H., 2015. Spatial observer-based repetitive controller: An active disturbance rejection approach. *Control Engineering Practice* 42, 1–11.
 Steinbuch, M., 2002. Repetitive control for systems with uncertain period-time. *Automatica* 38 (12), 2103–2109.
 Wang, Y., Gao, F., Doyle, F. J., 2009. Survey on iterative learning control, repetitive control, and run-to-run control. *Journal of Process Control* 19 (10), 1589–1600.
 Yao, W.-S., 2015. Adaptive repetitive control with two nonsynchronized sampling. *Journal of Dynamic Systems, Measurement, and Control* 137 (6), 061003/1–061003/8.
 Yao, W.-S., Tsai, M.-C., Yamamoto, Y., 2013. Implementation of repetitive controller for rejection of position-based periodic disturbances. *Control Engineering Practice* 21 (9), 1226–1237.
 Yu, S.-H., Hu, J.-S., 2000. Asymptotic rejection of periodic disturbances with fixed or varying period. *Journal of Dynamic Systems, Measurement, and Control* 123 (3), 324–329.